doi:10.3772/j.issn.1006-6748.2018.03.004

Application of improved back-propagation algorithms in classification and detection of scars defects on rails surfaces①

Shi Tian(石 甜), Kong Jianyi②, Wang Xingdong, Liu Zhao
(School of Machinery and Automation, Wuhan University of Science and Technology, Wuhan 430081, P. R. China)

Abstract

An experimental platform with bracket structures, cables, parallel computer and imaging system is designed for defects detecting on steel rails. Meanwhile, an improved gradient descent algorithm based on a self-adaptive learning rate and a fixed momentum factor is developed to train back-propagation neural network for accurate and efficient defects classifications. Detection results of rolling scar defects show that such detection system can achieve accurate positioning to defects edges for its improved noise suppression. More precise characteristic parameters of defects can also be extracted. Furthermore, defects classification is adopted to remedy the limitations of low convergence rate and local minimum. It can also attain the optimal training precision of 0.00926 with the least 96 iterations. Finally, an enhanced identification rate of 95% has been confirmed for defects by using the detection system. It will also be positive in producing high-quality steel rails and guaranteeing the national transport safety.

Key words: detection platform, steel rail, improved algorithm, defect classification, identification rate

0 Introduction

During the production process, accurate and efficient defects detection on steel rails is of great significance in improving track quality and guaranteeing transport safety. Up to now, many methods have been developed to detect defects on rails. Ref. [1] described an alternative current field measurement (ACFM) to detect breaking defects on rails. Ref. [2] adopted an infrared light for defect detection on heavy rails. Besides, manual observation, eddy current and magnetic leakage techniques have also been proposed for defects detection[3,4]. However, false detection is of common occurrence for inefficient manual observation. Low detection precision will be caused by infrared and eddy-current methods. Besides, some other techniques may be complex, costly, imprecise and inefficient for defects detection. Therefore, exploring an efficient, facile and accurate method to detect defects on rails is still a big challenge.

In recent years, machine vision technique[5,6] has gained growing popularity in detection fields for its real-time, non-contact and precise advantages. The most common back-propagation[7,8], radial basis function (RBF)[9,10], counter propagation[11,12] and feedback[13,14] neural networks have gained great attentions in industrial visual classifications and inspections. Among them, back-propagation network has advantages in reducing fuzzy edges and extracting more defects details. Meanwhile, it can also effectively weaken the noise interference to achieve better real-time computation than others for accurate defects classifications.

However, some limitations of low convergence rate and local minimum still exist in classical gradient descent algorithm for training back-propagation network. Meanwhile, some incomplete detection results are often seen. Besides, some external interferences and unobvious gray changes are also found when detecting complex defects in poor production conditions. Recent years have seen some improved back-propagation algorithms. Ref. [15] introduced a back-propagation algorithm with an adaptive learning rate to predict landslides deformation. But its experimental reliability was not significantly improved. Ref. [16] put forward an improved algorithm to analyze the data of light distribution in orchards by modifying weights and thresholds. But its convergence speed and application object were

① Supported by the National Natural Science Foundation of China (No. 51174151), the Key Scientific Research Project of Education Department of Hubei Province (No. D20151102), and the Key Scientific and Technological Project of Wuhan Technology Bureau (No. 2014010202010088).
② To whom correspondence should be addressed. E-mail: kjywust@163.com
Received on July 6, 2017

severely restricted.

Herein, on the basis of classical gradient descent algorithm, an improved back-propagation algorithm is developed to achieve accurate and real-time defects classifications, which is constructed by adding the self-adaptive learning rate and a momentum factor of 0.6. Meanwhile, an experimental platform is designed for defects detection on rails. To evaluate its detection efficiency, training iterations have been investigated. The edge details and characteristic parameters have also been extracted to assess positional accuracy and identification rates of this detection platform.

1 Classification methods of defects

Defects on rails mainly contain rolling scars, marks, scratches, folds and other types. These defects have abundant geometry features, depth information and gray characteristics. Hence, their classifications are far beyond linear scopes. Multi-layer back-propagation neural network with an input layer, an output layer and more hidden layers, can meet their classifications requirements. The characteristic parameters of defect images extracted by machine vision are set as the input data, which are outputted to nodes in next layer until the final output of classification gets results. To reduce errors between target and actual outputs, the classical gradient descent algorithm is always used for improving classification accuracy.

Neural network training is determined by adjusting weights and biases in signal forward-propagation and error back-propagation processes. In signal process, the input of unit i with iteration number n is set as $x_i(n)$. The output of unit j is set as $y_j(n)$, as shown in

$$y_j(n) = f_j\left(\sum_{i=0}^{N} w_{ij}(n)x_i(n)\right) = \frac{1}{1+\exp(-s_j(n))} \tag{1}$$

where N refers to inputting number, w_{ij} means weight function and f_j denotes sigmoid function.

In the error back-propagation process, the expected output is set as $d_j(n)$ and the error signal is set as $e_j(n)$, as shown in

$$e_j(n) = d_j(n) - y_j(n) \tag{2}$$

The mean square error is expressed as

$$\xi_{AV} = \frac{1}{N}\sum_{n=1}^{N}\left(\frac{1}{2}\sum_{j=1}^{M} e_j^2(n)\right) \tag{3}$$

where M refers to outputting number and N represents the total number of training samples. The correction of weight w_{ij} is

$$\Delta w_{ij}(n) = -\eta\frac{\partial\xi(n)}{\partial w_{ij}} = -\eta\delta_j(n)x_i(n) \tag{4}$$

where negative sign means the gradient descent direction and the local gradient function is given as

$$\delta_j(n) = e_j f_j'(s_j(n)) \tag{5}$$

The classical gradient descent algorithm for training neural network is found with some limitations of low learning efficiency, low convergence rate and local minimum. Herein, an improved gradient descent algorithm is developed by adding self-adaptive learning rate and momentum factor to remedy these limitations. After being added with momentum factors, the correction of weight is

$$\Delta w_{ij}(n+1) = \eta\delta_j x_i(n) + m_c\Delta w_{ij}(n) \tag{6}$$

where m_c refers to momentum factors with value range from 0.01 to 1.00. As shown in Eq. (6), added momentum factors can adjust the weight towards an average direction of the error-surface bottom. When the weight goes into a flat area of the error-surface bottom, δ_j will be very small and $\Delta w_{ij}(n+1)$ is close to Δw_{ij}, which can effectively prevent the occurrence of $\Delta w_{ij} = 0$. As a result, it can help the network jump out of the local minimum value of the error-surface bottom.

Another important reason for the slow convergence rate of algorithm is improper selection of learning rates. The learning rate $l_{r(t)}$ is expressed as

$$l_{r(t)} = l_{r(t-1)}\left(1 - \frac{t}{T+C}\right) \tag{7}$$

where t refers to iterations, T means total iterations and C represents iteration constant. A small learning rate can lead to a slow convergence rate. A large learning rate can cause oscillation and divergence. Hence, improved convergence speed and calculation accuracy can be achieved with the appropriate choice of learning rates.

2 Experimental platform

2.1 Detection system

The experimental platform for defects detection is exhibited in Fig. 1(a). It mainly consists of imaging system, parallel computers, bracket structures and cable system. Among the imaging system, Dalsa SG-01k40 and Computar M5018-MP are chosen as the models of linear CCD cameras and lens, respectively. The camera layout is exhibited in Fig. 1(b). The most frequent defects are always found on the camber surface of rail waist. Hence, cameras 2, 3, 5 and 6 are set to focus on such camber surface. Camera 1 and 4 are set to focus on the top and bottom surfaces. Such layout of cameras can collect more comprehensive images on rail surfaces. The structural design of light source is shown in Fig. 1(c). 8 rectangular LED light sources are connected by expansion links and hinges. Such layout of

light sources can make uniform illumination on rail surfaces.

The imaging system is installed on gantry brackets. Defects images are firstly achieved by sliding brackets on guide rails. Then image signals are processed by transmitting to parallel computers. After that, defects detection and recognition results will be obtained.

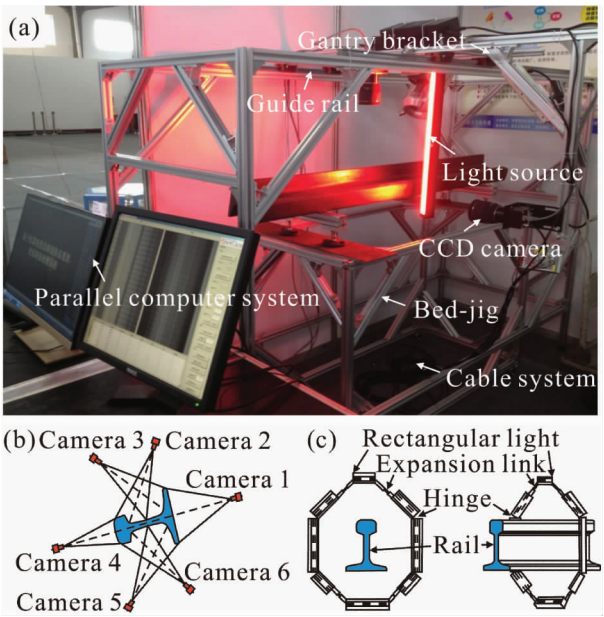

(a) Experimental platform, (b) Cameras layouts, (c) Light sources layouts

Fig. 1 Defect detecting platform

2.2 Calibration of pixel response nonuniformity

In the working process of CCD cameras, energy exchanges between photons and silicon atoms can promote the output of charge packets. Then the packets further convert to current or voltage signals to obtain resultant photoelectric information. Generally, a linear relation is found between pixel charges (Y) and irradiances (X) in Eq. (8):

$$Y = AX + B \tag{8}$$

where A refers to relational parameter determined by irradiation frequency and B denotes charge changes caused by interference noises. However, due to the existence of dark currents and external noises, the pixel response nonuniformity of cameras can be found in image acquisition process. As a result, some unwanted errors between gray values of each pixel can be caused in the case of a fixed light irradiance. To ensure that all gray values are calculated within an allowable error range, photoelectric responses must be calibrated.

Herein, the outputting charge of a certain pixel C is deemed as an observed target gray value Y_C in Eq. (9). By synthetically considering Eq. (8) and Eq. (9), the revised gray scale of pixel $C(*Y_C)$ is finally obtained in Eq. (10):

$$Y_C = A_C X_C + B_C \tag{9}$$

$$*Y_C = A(Y_C - B_C)/A_C + B \tag{10}$$

By adjusting the current values of light sources, various irradiation intensities are attained. Fig. 2(a) exhibits the recorded gray values of different irradiances for various pixels. Obviously, an increasing gray scale deviation is seen with the enhancement of irradiances. Take pixel 200 as an example, its target gray values Y_{200} versus irradiation intensities X_{200} is linearly fitted in Eq. (11). Fig. 2(b) shows the average gray values of each pixel with different irradiances. A proportional relationship is found between gray values and irradiances after linear fitting, as exhibited in Fig. 2(c) and Eq. (12). When the irradiance is 80 nW. cm^{-2} ($Y_{200} = 180$), the revised gray of pixel 200 ($*Y_{200}$) is 186.664 according to Eq. (10). Fig. 2(d) shows the calibrated gray values for various irradiances, among which a lower gray value deviation is seen compared with the unregulated one. Fig. 3 exhibits a scar image before and after the calibration of pixel response nonuniformity. Clearly, an undistorted defect image with considerably decreased noises has been extracted after the calibration process.

$$Y_{200} = 2.092X_{200} + 10.499 \tag{11}$$

$$Y = 2.132X + 13.923 \tag{12}$$

It is known that rail surfaces have certain radians. When extracting defects images on rails, some uneven background illuminations inevitably exist due to various

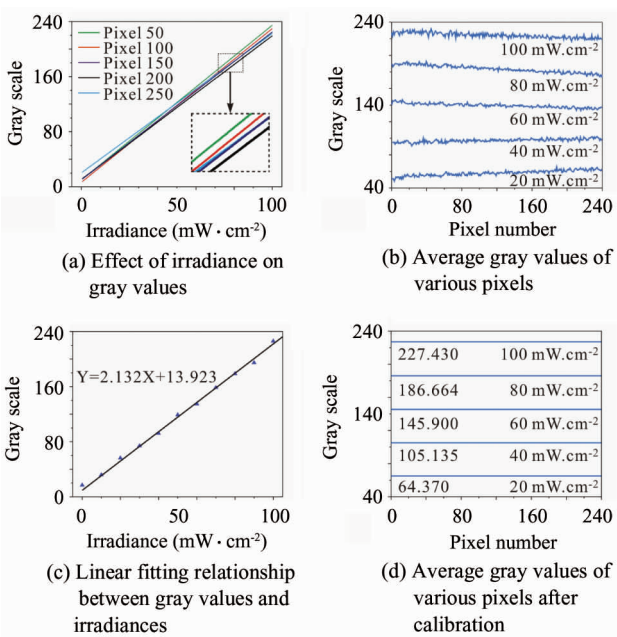

Fig. 2 Calibration of pixel response nonuniformity of CCD cameras

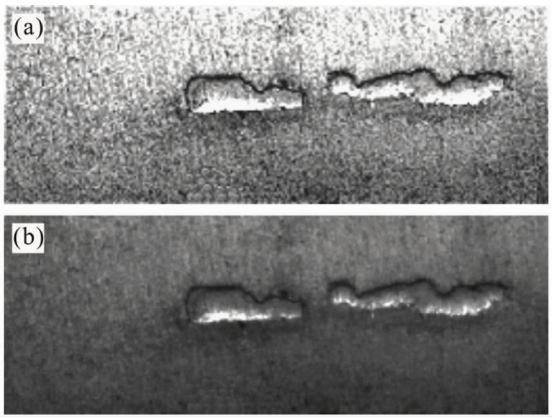

(a) Before calibration of pixel response nonuniformity
(b) After calibration of pixel response nonuniformity

Fig. 3 Scar images

shooting angles of cameras and beam-angles of light sources, as shown in Fig. 4(a), Fig. 4(b) exhibits the corresponding background light of the scar image achieved by MATLAB. To intuitively characterize its background details, a three-dimensional simulation with gray scales is conducted in Fig. 4(e). Clearly, uneven light distributions are seen. To eliminate these uneven illuminations, the process of background subtraction is conducted. And the resultant scar image is exhibited in Fig. 4(c). Meanwhile, the corresponding background light and three-dimensional gray scales are shown in Fig. 4(d) and Fig. 4(f), respectively. Clearly, more uniform light distributions are seen on the processed scar image, which can help to achieve more integrated and precise edge detection in the following step.

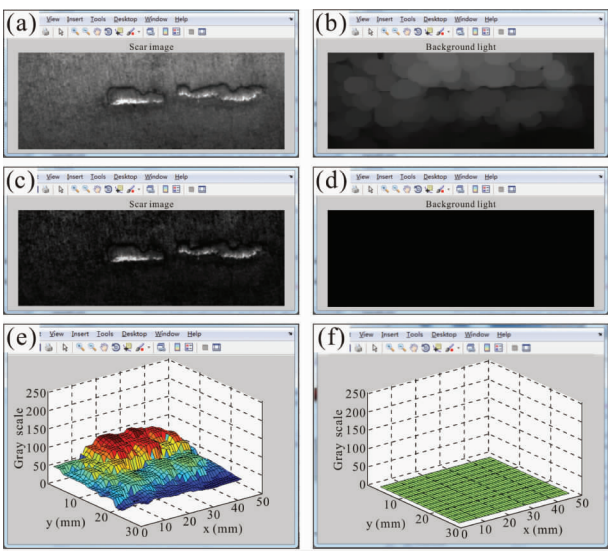

(a) Scar image, (b) Background light of scar image, (c) Scar image after calibration, (d) Background light of scar image after calibration, (e) Three-dimensional gray scales of scar image, (f) Three-dimensional gray scales of scar image after calibration

Fig. 4 Calibration of uneven background illuminations

3 Detection and classification results

3.1 Edge detection results

The classical Sobel operator is used to extract edge details on scar defect, as shown in Fig. 5. Clearly, comprehensive and continuous edge details including edge position data (see Table 1) have been extracted, which can distinctly and precisely characterize the defect features. Meanwhile, such operator can easily achieve accurate location to defects and then extract precise characteristic parameters. Besides, the noise points are seldom seen suggesting that the operator can help to identify and judge defect edge information for its excellent noise suppression.

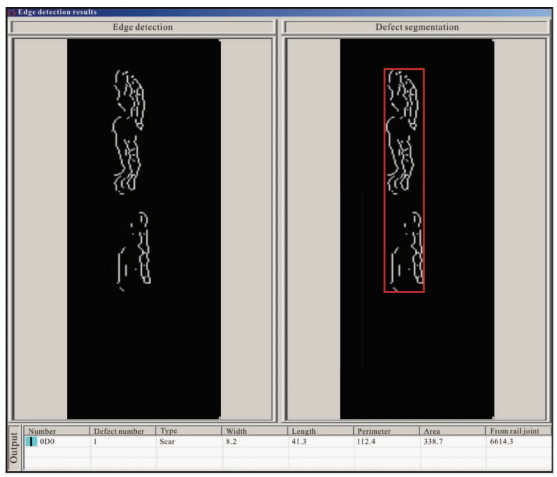

Fig. 5 Edge image of scar defect

The classification and identification of surface defects on rails are conducted by parallel computers. The extraction of characteristic parameters can be achieved by converting the physical features of a defect into some digital features that can only be processed by computers. Hence, accurate extraction of characteristic parameters acts as a fundamental role in defects classification and identification. After the binary and segmentation processes of the scar image, 24 sets of characteristic parameters are extracted, as shown in Table 2. These digital parameters can reflect important physical features of the scar defect.

Table 1 Edge position information of scar defect

Position parameter	Width(mm)	Length(mm)	Perimeter(mm)	Area(mm^2)	From rail joint(mm)
value	8.2	41.3	112.4	338.7	6614.3

Table 2 Characteristic parameters of scar defect

Characteristic	Value	Characteristic	Value	Characteristic	Value	Characteristic	Value
Dispersity	69.75	Gray entropy	7	Background energy	0.6	Second moment invariants	12.43
Rectangle degree	0.72	Average background gray	69	Background homogeneity	0.96	Third moment invariants	23.82
Aspect ratio	0.18	Background gray codomain	255	Relevance	0.2	Fourth moment invariants	25.44
Average gray	95	Background gray variance	23	Energy	0.6	Fifth moment invariants	49.35
Gray codomain	224	Background gray entropy	6	Homogeneity	0.96	Sixth moment invariants	30.84
Gray variance	53	Background correlation	0.08	First moment invariants	5.99	Seventh moment invariants	49.29

3.2 Neural network classification

Herein, back-propagation neural network with excellent self-learning and self-organizing ability has been adopted to achieve accurate and rapid classification of defects on rails. When it comes to neuron numbers in each layer, 24 sets of characteristic parameters (see Table 2) are extracted as the input data. The neuron numbers in two hidden and one output layers are respectively set as 15, 4 and 4 for the highest correlation coefficient and the lowest error between target and actual outputs. Based on above analyses, the optimized network structure is determined, as shown in Fig. 6. In such network, sigmoid and purelin functions are used as transfer functions in hidden and output layers, respectively. To test the classification effect, 40 sets of scar images are obtained by the designed image acquisition system. Among them, 20 sets are used as training specimens and the others as testing specimens. The maximum training frequency, minimum mean square error (MSE) and learning step are set as 500, 0.01 and 0.15, respectively. During the simulation process, the iteration will stop and the system will converge immediately when MSE falls below 0.01 or iteration reaches to 500.

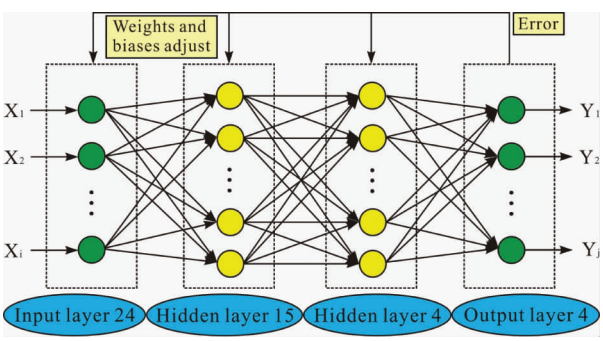

Fig. 6 Structure of back-propagation neural network

Fig. 7 shows various neural network training curves for detects classifications. Fig. 7(a) exhibits the training curve with classical gradient descent algorithm (algorithm a). As seen, after iteration for 500 times with 10193ms, MSE is 0.343, which is larger than the convergent value of 0.01. The training curve attained by using an improved gradient descent algorithm with an additional m_c of 0.6 is seen in Fig. 7(b) (algorithm b). However, after iteration for 500 times with 8832ms, the corresponding MSE is 0.228, which is still larger than the convergent value. Fig. 7(c) depicts another training curve by adopting an improved algorithm with a self-adaptive l_r (algorithm c). Clearly, its MSE can attain the optimal training precision of 0.00996 (<0.01) with 158 iterations and 5057ms. The training curve obtained by using an improved algorithm with a fixed learning rate ($l_r = 0.15$) and a fixed momentum factor ($m_c = 0.6$) is shown in Fig. 7(d) (algorithm d). Its MSE can reach the optimal training precision of 0.00989 (<0.01) with 105 iterations and 3692ms. Fig. 7(e) describes a training curve by using an improved gradient descent algorithm with a self-adaptive l_r and a fixed m_c of 0.6 (algorithm e). Clearly, its MSE can achieve the optimal training precision of 0.00926 (<0.01) with the least 96 iterations and 1921ms. It can be seen from Fig. 7(f) that algorithm e can achieve the training accuracy with the least iterations. The reason for this is that such improved algorithm can overcome some limitations of the classical algorithm, such as low convergence rate, strong coupling relation with other parameters and local minimum. Hence, the above improved algorithm can improve both the classification efficiency and recognition rate of defects.

To further determine the optimal m_c, a series of training curves for defects classifications with various m_c

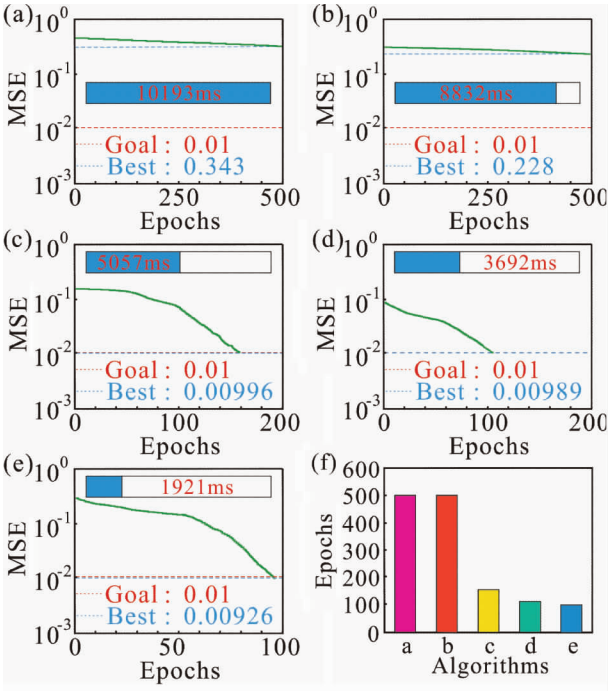

(a) Classical algorithm, (b) Improved algorithm with an m_c of 0.6, (c) Improved algorithm with a self-adaptive l_r, (d) Improved algorithm with an l_r of 0.15 and an m_c of 0.6, (e) Improved algorithm with a self-adaptive l_r and an m_c of 0.6, (f) Contrastive iterations of the above five algorithms

Fig. 7 Neural network training curves by using various gradient descent algorithms

have been measured, as shown in Fig. 8. Obviously, the mean square errors based on various algorithms with fixed m_c of 0.2, 0.4, 0.6, 0.8 and 1.0 can achieve the optimal training precision with 152, 144, 96, 308 and 500 iterations, respectively. Take full account of the above iterations, the gradient descent algorithm based on a self-adaptive l_r and a fixed m_c of 0.6 can overcome the limitations of the classical algorithm, which accounts for its best classification efficiency.

To further investigate the effect of l_r on improved algorithms under the optimal m_c of 0.6, a series of training curves for defects classifications with various l_r have been measured, as shown in Fig. 9. Clearly, the mean square errors based on various algorithms with fixed l_r of 0.05, 0.10, 0.15, 0.20 and 0.25 can reach the optimal training precision with 117, 109, 105, 113 and 147 iterations, respectively. Therefore, the gradient descent algorithm based on a fixed l_r of 0.15 can achieve the best classification efficiency. It is also concluded that the classification efficiency of all fixed l_r is still lower than the self-adaptive one only with 96 iterations. Hence, algorithm e based on a self-adaptive l_r and a fixed m_c of 0.6 is used in this work to train the network.

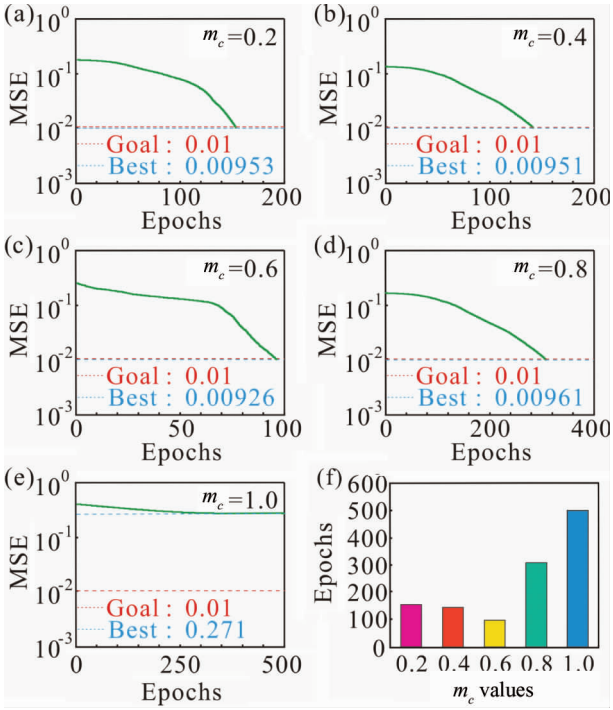

(a) m_c = 0.2, (b) m_c = 0.4, (c) m_c = 0.6, (d) m_c = 0.8, (e) m_c = 1.0, (f) Contrastive iterations for various m_c

Fig. 8 Neural network training curves based on various momentum factors

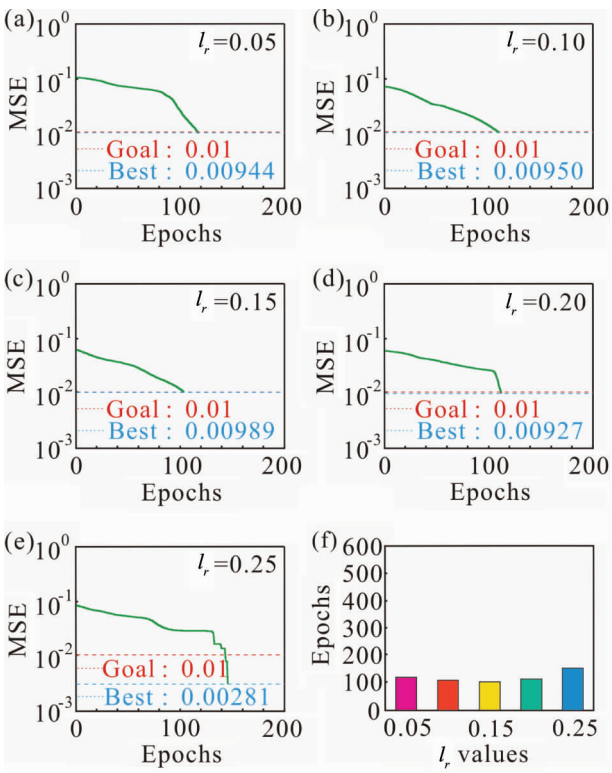

(a) l_r = 0.05, (b) l_r = 0.10, (c) l_r = 0.15, (d) l_r = 0.20, (e) l_r = 0.25, (f) Contrastive iterations for various l_r

Fig. 9 Neural network training curves based on various learning rates

3.3 Recognition accuracy analysis

Table 3 shows the output data of the testing specimens (20 sets) after being processed with algorithm e. The output value will be identified as 1 if it is larger than 0.5. Otherwise, it will be regarded as 0. Namely, an output result (0, 1, 0, 0) with 4 parameters can be recognized as a scar defect. Clearly, the recognition number of scar defects based on algorithm e is 19.

Table 3 The output data of the testing specimens (20 sets) after being processed with algorithm e

Specimen	Output value	Discriminant result
1	(0.0485, 0.9794, 0.0943, 0.0931)	(0,1,0,0)
2	(0.1249, 0.9774, 0.0983, 0.0025)	(0,1,0,0)
3	(0.0811, 0.9451, 0.0593, 0.0183)	(0,1,0,0)
4	(0.0173, 0.9096, 0.0443, 0.0477)	(0,1,0,0)
5	(0.0202, 0.9547, 0.1822, 0.0188)	(0,1,0,0)
6	(0.0055, 0.0093, 0.0624, 0.0264)	(0,0,0,0)
7	(0.1854, 0.9873, 0.0374, 0.0249)	(0,1,0,0)
8	(0.1753, 0.9836, 0.0382, 0.0066)	(0,1,0,0)
9	(0.1077, 0.9765, 0.0306, 0.0073)	(0,1,0,0)
10	(0.0902, 0.9675, 0.0099, 0.0605)	(0,1,0,0)
11	(0.0029, 0.9508, 0.0389, 0.0623)	(0,1,0,0)
12	(0.0925, 0.9582, 0.0203, 0.0627)	(0,1,0,0)
13	(0.0388, 0.9473, 0.0490, 0.0903)	(0,1,0,0)
14	(0.0529, 0.9794, 0.0094, 0.0716)	(0,1,0,0)
15	(0.0905, 0.9520, 0.0172, 0.0095)	(0,1,0,0)
16	(0.1302, 0.9708, 0.0285, 0.0927)	(0,1,0,0)
17	(0.0040, 0.9428, 0.1003, 0.0091)	(0,1,0,0)
18	(0.0127, 0.9471, 0.0491, 0.0740)	(0,1,0,0)
19	(0.0921, 0.9710, 0.0089, 0.1001)	(0,1,0,0)
20	(0.0193, 0.9737, 0.0452, 0.0072)	(0,1,0,0)

Fig. 10 shows various recognition results of scar defects after being processed with other algorithms. Clearly, the correct recognition number based on algorithm a, b, c and d are 12, 13, 15 and 16, respectively. Furthermore, the defect identification rate can be calculated as

$$r = n/m \tag{13}$$

where r refers to defect identification rate, n means correct recognition number and m denotes testing number ($m = 20$). Accordingly, algorithm e has got the optimal defect identification rate of 95%, higher than others. According to these analyses, the designed experimental platform with the improved gradient descent algorithm based on a self-adaptive l_r and a fixed m_c of 0.6 can detect surface defects on heavy rails with higher accuracy and efficiency.

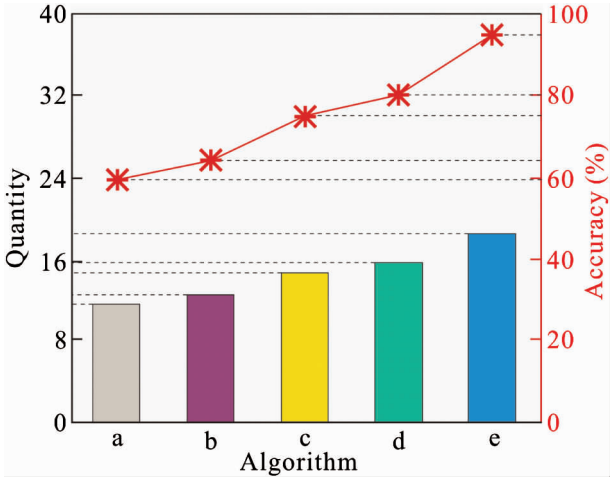

Fig. 10 Recognition quantity and recognition accuracy of scar defects for various algorithms

4 Conclusions

An experimental platform is designed for scar defects detection on rails surfaces. The pixel response nonuniformity and uneven background illuminations have been calibrated during the imaging process. In the detection system, an improved gradient descent algorithm based on a self-adaptive learning rate and a fixed momentum factor of 0.6 is proposed to comprehensively consider accuracy, efficiency and classification efficiency of defects. Detection results show that accurate positioning of defects with complete edge information is easily attained for its noise suppression capacity. Meanwhile, more precise characteristic parameters are extracted to achieve convergent precision with the least 96 iterations. And also the optimal defect identification rate of 95% is found for the detection system. Parameters and structures optimization of the experimental platform and more effective gradient descent algorithms are hoped to be solved and designed in future work.

References

[1] Munoz J M C, Márquez F P G, Papaelias M. Railroad inspection based on ACFM employing a non-uniform B-spline approach[J]. *Mechanical Systems and Signal Processing*, 2013, 40(2): 605-617

[2] Mi Z Z, Xie Z J. Theoretical and experimental research on the defects of hot rolled heavy rail[J]. *Metalurgia International*, 2012, 17(9): 221-225

[3] Helena G R, Tiago R, Jakub K, et al. An SVM approach with electromagnetic methods to assess metal plate thickness[J]. *Measurement*, 2014, 54(8): 201-206

[4] Khodayari-rostamabad A, Reilly J P, Nikolova N K, et al. Machine learning techniques for the analysis of magnetic flux leakage images in pipeline inspection[J]. *IEEE Transactions on Magnetics*, 2009, 45(8): 3073-

3084
[5] Nashat S, Abdullah A, Abdullah M Z. Machine vision for crack inspection of biscuits featuring pyramid detection scheme[J]. *Journal of Food Engineering*, 2014, 120(1): 233-247
[6] Makky M, Soni P. Development of an automatic grading machine for oil palm fresh fruits bunches (FFBs) based on machine vision[J]. *Computers & Electronics in Agriculture*, 2013, 93(2): 129-139
[7] Zhang K Z, Tian W F, Feng Q. Combination of distributed Kalman filter and BP neural network for ESG bias model identification[J]. *Transactions of Nanjing University of Aeronautics and Astronautics*, 2010, 27(3): 226-231
[8] Yu J B, Zhou X L, Deng C L, et al. Optimization of injection molding process of bearing stand based on BP network method[J]. *Transactions of Nanjing University of Aeronautics and Astronautics*, 2014, 31(2): 190-195
[9] Li D X, Feng P F, Zhang J F, et al. Calculation method of convective heat transfer coefficients for thermal simulation of a spindle system based on RBF neural network [J]. *The International Journal of Advanced Manufacturing Technology*, 2014, 70(5): 1445-1454
[10] Niu H L, Wang J. Financial time series prediction by a random data-time effective RBF neural network[J]. *Soft Computing*, 2014, 18(3): 497-508
[11] Nikola M, Spela Z, Viktor D, et al. Assessment of applicability domain for multivariate counter - propagation artificial neural network predictive models by minimum Euclidean distance space analysis: A case study[J]. *Analytica Chimica Acta*, 2013, 759: 28-42
[12] Waqas H B, Jamil A, Imran S, et al. A forward only counter propagation network-based approach for contraceptive method choice classification task[J]. *Journal of Experimental and Theoretical Artificial Intelligence*, 2012, 24(2): 1-9
[13] Dai S L, Wang M, Wang C, et al. Learning from adaptive neural network output feedback control of uncertain ocean surface ship dynamics[J]. *International Journal of Adaptive Control & Signal Processing*, 2014, 28(3-5): 341-365
[14] Yu Z, Li S. Neural-network-based output-feedback adaptive dynamic surface control for a class of stochastic nonlinear time-delay systems with unknown control directions [J]. *Neurocomputing*, 2014, 129(5): 540-547
[15] Ran Y, Xiong G, Li S, et al. Study on deformation prediction of landslide based on genetic algorithm and improved BP neural network[J]. *Kybernetes*, 2010, 39(8): 1245-1254
[16] Hu J, Zhou G, Xu X. Using an improved back propagation neural network to study spatial distribution of sunshine illumination from sensor network data[J]. *Ecological Modelling*, 2013, 266(1): 86-96

Shi Tian, born in 1988. She is currently carrying on a successive postgraduate and doctoral program in School of Machinery and Automation, Wuhan University of Science and Technology. She received the B. S. degree in Wuhan University of Science and Technology in 2012. Her research interests include defects detection technology, machine vision technology, neural network technology and computer technology.